Stability Factors F_c, F_s, and F_γ for Twin Tunnels in Three Dimensions

Jim Shiau[1] and Fadhil Al-Asadi[2]

Abstract: This paper aims to study the three-dimensional (3D) tunnel heading pressure of twin circular tunnels in a drained cohesive–frictional soil using a stability factor approach and finite-element limit analysis (FELA). The primary concept adopted will be the use of a conventional equation that is similar to the traditional bearing capacity factors (e.g., N_c, N_s, and N_γ) in Terzaghi's bearing capacity equation. For various spacing ratios (S/D) between the tunnels, the stability of the tunnels is expressed in terms of nondimensional tunnel stability factors (e.g., F_c, F_s, and F_γ), which are functions of the depth ratio (C/D) and soil internal friction angle (ϕ). For conciseness, the results will be presented in charts and tables with the tunnel stability factors that used the rigorous FELA upper (UB) and lower bound (LB) solutions.
DOI: 10.1061/(ASCE)GM.1943-5622.0002264.

Author keywords: Upper bound; Lower bound; Three-dimensional finite-element limit analysis; Tunnel stability factors; Spacing ratio.

Introduction

Limit equilibrium methods and limit analysis methods are widely used to study tunnel stability in drained cohesive–frictional soil. Horn (1961) proposed a limit equilibrium model to assess stability under drained conditions at the tunnel face. Horn's wedge model was improved by Anagnostou and Kovári (1996) to calculate the limit support pressure in a homogeneous drained soil. The analytical upper bound (UB) method was used by Atkinson and Potts (1977) to study the critical tunnel pressure for an unlined shallow circular tunnel in sand. An improved UB mechanism was proposed by Leca and Dormieux (1990) that used conical-shaped rigid blocks. Mollon et al. (2009, 2010, 2011, 2013) further proposed new rigid block failure mechanisms by assuming different shapes of the failure zone in front of the tunnel face, and their numerical solutions have been improved significantly. The previous studies were limited to shallow tunnels and are based on the analytical UB theorem that requires assumptions of various failure mechanisms. Recently, Zhang et al. (2015, 2020) and Li and Zhang (2020) studied face stability and anisotropic sands in shallow tunnels with advanced three-dimensional (3D) numerical analyses. Ukritchon et al. (2017, 2020) studied undrained stability with UB and lower bound (LB) limit analysis that considered nonhomogeneous clays. For deep tunnels, very few results have been reported due to the difficulty in selecting appropriate 3D rigid blocks (Shiau and Al-Asadi 2020a, b, 2021).

For twin circular tunnel stability, Ghaboussi and Ranken (1977) used a two-dimensional (2D) displacement-based finite-element method to study the interaction effects on the construction of parallel tunnels. Wu and Lee (2003) studied the soil movements above the tunnel and the associated collapse mechanisms using centrifuge models. Most critical stability does not always occur at the smallest spacing between the tunnels.

Following Wu and Lee (2003), Lee et al. (2006) experimentally studied the excess pore water pressure generation, ground surface settlement, soil arching, and tunnel stability in soft clay.

Osman (2010) evaluated twin tunnels overlapping effects using UB solutions and determine the internal pressure required to resist the collapse for various depths and spacing between tunnels. Stability charts for twin unlined circular tunnels were produced by Sahoo and Kumar (2015) using an LB method. The undrained stability of dual circular and square tunnels was studied by Wilson et al. (2014, 2015) using finite-element limit analysis (FELA). They reported that the stability was lowest when the twin tunnels are approximately 1.5 times the tunnel widths apart.

Of note, very few studies have been reported on 3D twin tunnels stability that used the stability factors approach. Shiau and Al-Asadi (2020c, d, f) adopted a stability factor approach that used the FELA technique, analogous to the classic bearing capacity equation, to calculate the minimum supporting pressure (σ_t), as shown in

$$\sigma_t = -cF_c + \sigma_s F_s + \gamma D F_\gamma \tag{1}$$

where c = soil cohesion; σ_s = surcharge pressure; γ = unit weight of the soil; D = tunnel diameter; and the stability factors F_c, F_s, and F_γ = functions of the depth ratio (C/D) and the soil friction angle (ϕ). This paper follows the work of Shiau and Al-Asadi (2020c, d, f), and aims to produce rigorous UB and LB solutions for the tunnel stability factors (F_c, F_s, and F_γ) for various spacing ratios (S/D) between the tunnels. This paper provides a simple and accurate design tool for practicing engineers to compute the minimum inner support pressure of twin circular tunnels in cohesive–frictional soils.

3D Twin Headings and FELA Modeling

The center-to-center distance (S) plays a key role in 3D twin tunnel stability. When the distance (S) is small, the stress field around each tunnel overlaps and the interactions between the tunnels become important in stability design. The 3D problem statement with S is shown in Fig. 1. The ground is modeled as a uniform Mohr–Coulomb material with c, ϕ, and γ. The tunnels have a cover

[1]Associate Professor, School of Civil Engineering and Surveying, Univ. of Southern Queensland, Toowoomba, QLD 4350, Australia (corresponding author). ORCID: https://orcid.org/0000-0002-9220-3184. Email: jim.shiau@usq.edu.au

[2]Ph.D. Student, School of Civil Engineering and Surveying, Univ. of Southern Queensland, Toowoomba, QLD 4350, Australia.

Note. This manuscript was submitted on January 6, 2021; approved on October 11, 2021No Epub Date. Discussion period open until 0, 0; separate discussions must be submitted for individual papers. This paper is part of the ***International Journal of Geomechanics***, © ASCE, ISSN 1532-3641.

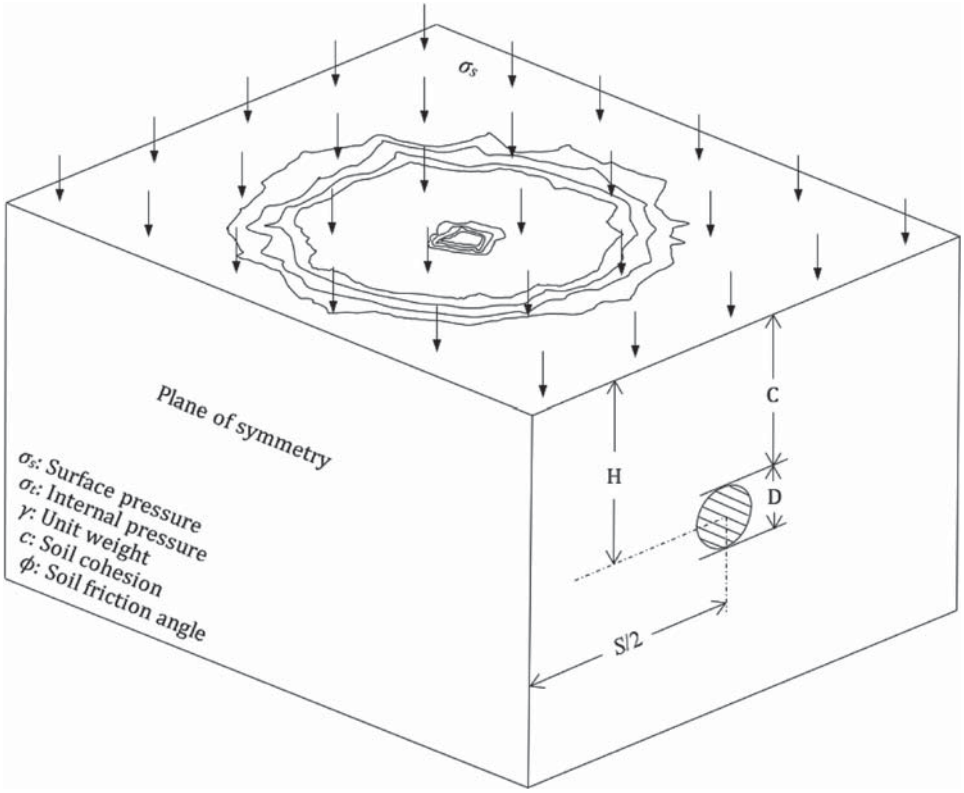

Fig. 1. Problem definition [symmetrical domain for a large S/D ($S/D = 8$)].

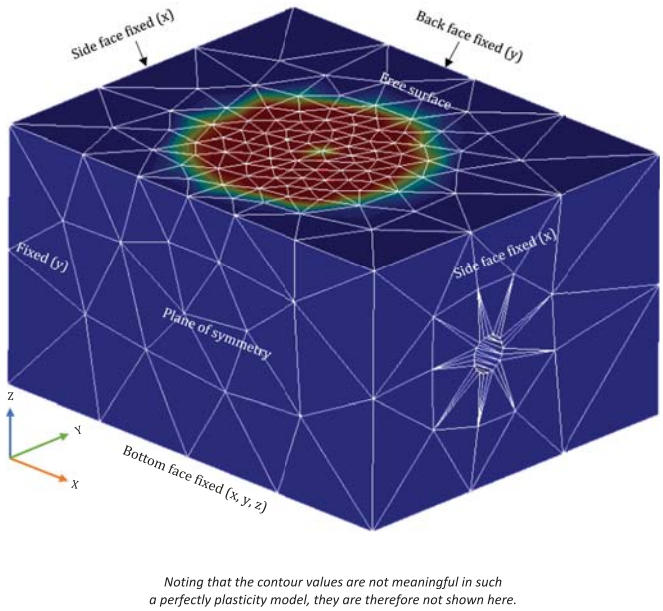

Fig. 2. Typical adaptive mesh with boundary conditions and failure mechanism plot that shows a single tunnel response (e.g., half domain, $\phi = 0°$, $C/D = 3$, and $S/D = 8$).

depth (C) and a diameter (D) above the crown of the tunnel and are separated by S. The surcharge applied to the ground surface is σ_s and the internal tunnel pressure is σ_t. As shown in Fig. 1, the problem of twin tunnels is symmetrical about the centerline of the distance between the tunnels centers.

A typical FELA adaptive half mesh and boundary condition used in this study is shown in Fig. 2 (e.g., $C/D = 3$ and $S/D = 8$). The ground surface and the 3D heading surface (not visible in the current 3D plot) were not constrained to move. The side surfaces were restricted to move in the x-direction (normal direction). The same condition was applied to the front and the back surfaces of the model, that is, they were allowed to move in the y-direction (normal direction). The nodes on the bottom surface were not allowed to move in any direction. To represent a smooth interface condition, the nodes on the tunnel lining, although not visible in the current 3D plot, were not allowed to move in the normal direction.

It was important to choose a large model size. This ensured that the entire velocity field developed within the 3D domain and that the failure mechanism did not pass through the model boundaries. Fig. 2 shows an example plot of the symmetrical model for a large S/D (e.g., $C/D = 3$ and $S/D = 8$). Since the plot is for a large S/D, the ground failure area resembles a perfectly circular shape, which is similar to a single tunnel response. However, Fig. 3 shows a closely spaced twin tunnel (e.g., $C/D = 3$ and $S/D = 4$). The surface failure area is close to an elliptical shape due to the small spacing between the tunnels. Of note, the contour values were not meaningful in such a perfectly plasticity model; therefore they are not shown.

The adaptive mesh technique was employed to enable accurate limit loads to be obtained using a bounds gap error estimator (Sloan 2013). In practice, the solutions are more valuable when UBs are accompanied by LBs; therefore, the exact solution can be bracketed from above and below. Three iterations of adaptive meshing based on shear dissipation criteria were used. The adaptive FELA program (OptumCE 2019) has been widely used to determine the limit load of 2D and 3D problems with the power of finite-element discretization and the bounding capability of LBs and UBs plastic limit theorems. In addition, it has been successfully applied to solve various stability problems with underground stability (Shiau et al. 2016; Shiau and Sams 2019; Shiau and Hassan 2020; Shiau and

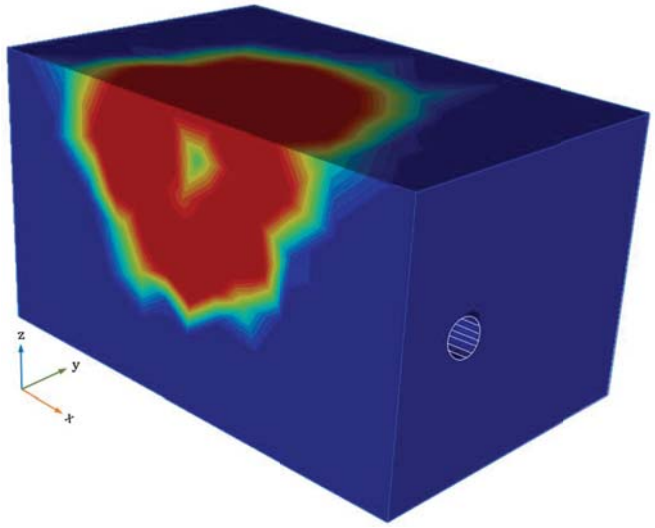

Fig. 3. Failure mechanism plot that shows twin tunnels effect (e.g., half domain, $\phi = 0$, $C/D = 3$, and $S/D = 4$).

Al-Asadi 2018, 2020a, b, c, d, e, f; Shiau et al. 2021a, b). For details on the theoretical UB and LB formulations refer to Sloan (2013).

A total of 27,666 FELA analyses were studied to determine the stability factors (e.g., F_c, F_s, and F_γ). These factors are functions of the S/Ds ($S/D = 2$–28), C/Ds ($C/D = 2$–10), and ϕ ($\phi = 0°$–$40°$). For each combination of parameters, σ_t optimized the UB and LB simulations to compute the bound solution of the stability factors (e.g., F_c, F_s, and F_γ). The procedures involved in the calculations of the three factors are as follows:

1. Eq. (1) reduces to $\sigma_t = -cF_c$ when $\gamma = 0$ and $\sigma_s = 0$. F_c can then be computed with known values of c and σ_t.
2. Eq. (1) reduces to $\sigma_t = \sigma_s F_s$ when $\gamma = 0$ and $c = 0$. F_s can then be estimated with known values of σ_s and σ_t.
3. Eq. (1) reduces to $\sigma_t = \gamma D F_\gamma$ when $c = 0$ and $\sigma_s = 0$. F_γ can be computed with known values of γ, D, and σ_t.

With the complete twin tunnel stability factors, the tunnel support pressure can be estimated using Eq. (1).

Discussing the Twin Tunnel Stability Factors

3D FELA were performed to calculate the UB and LB limits of the stability factors (e.g., F_c, F_s, and F_γ) for various C/D ($C/D = 2$–10), S/D ($S/D = 2$–28), and ϕ ($\phi = 0°$–$40°$). The effects of the parameters (C/D, S/D, and ϕ) on the tunnel stability factors (F_c, F_s and F_γ) are shown in Figs. 4–6 and 8–18.

F_c, F_s, and F_γ in an Undrained Condition

Of note, F_c is a function of the C/D and S/D, Fig. 4 shows that F_c increased nonlinearly as S/D increased until it reached a constant value. At this point, F_c is at its maximum value, and the twin tunnels stability is unaffected by the tunnel spacing. The corresponding S/D is a critical S/D that separates twin tunnels [the minimum spacing ratio $(S/D)_{\min}$].

As shown in Fig. 5, F_s has a constant value of unity irrespective of values of C/D and S/D. Of interest, for soils in an undrained condition ($\phi = 0$), the stability is independent of the loading direction due to zero volume loss during plastic shearing (Shiau and Sams 2019).

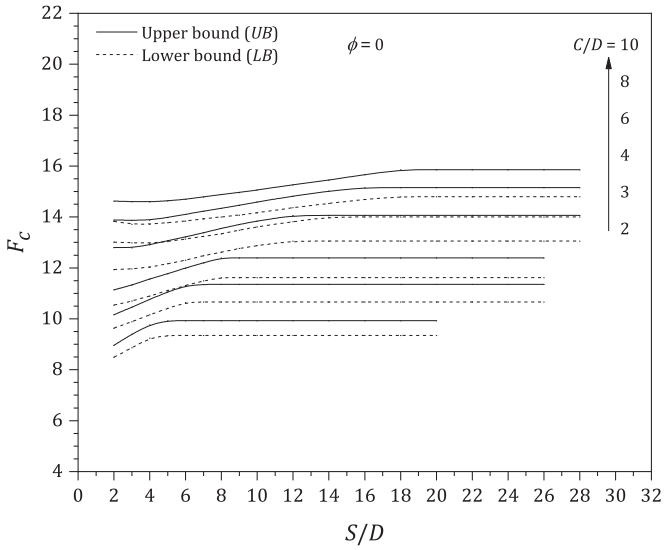

Fig. 4. 3D F_c versus S/D and various C/D ($\phi = 0°$).

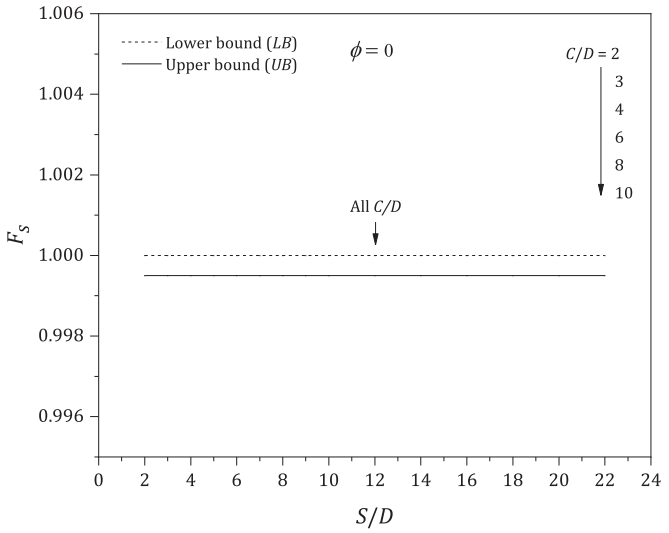

Fig. 5. 3D F_s versus S/D and various C/D ($\phi = 0°$).

As shown in Fig. 6, F_γ is independent of S/D and is only a function of C/D. The unit weight effect is the same as the surcharge effect. The only difference is that $F_\gamma = (C/D + 0.5)$ for all values of S/D. The larger the C/D value is, the larger F_γ is. This finding agrees with results in the literature (Shiau and Al-Asadi 2020c, d) for single tunnels.

The 3D $(S/D)_{\min}$ for various C/D is shown in Fig. 7. A linear relationship was observed between C/D and $(S/D)_{\min}$ for $\phi = 0$. When a design spacing ratio is $<(S/D)_{\min}$, the twin tunnel interaction effects must be studied. When $S/D \geq (S/D)_{\min}$, the stability of each of the tunnels is essentially identical to those of the corresponding single tunnel. In addition, the 3D results of $(S/D)_{\min}$ for various C/D, which are shown in Fig. 7, can be calculated using

$$(C/D)_{\min} = 1.8 \times (C/D) + 1.0 \tag{2}$$

Of note, the conservative 2D results obtained in Shiau and Al-Asadi (2020e) indicated a larger gradient of the linear envelope. The results in Sahoo and Kumar (2015) agreed reasonably well with the others.

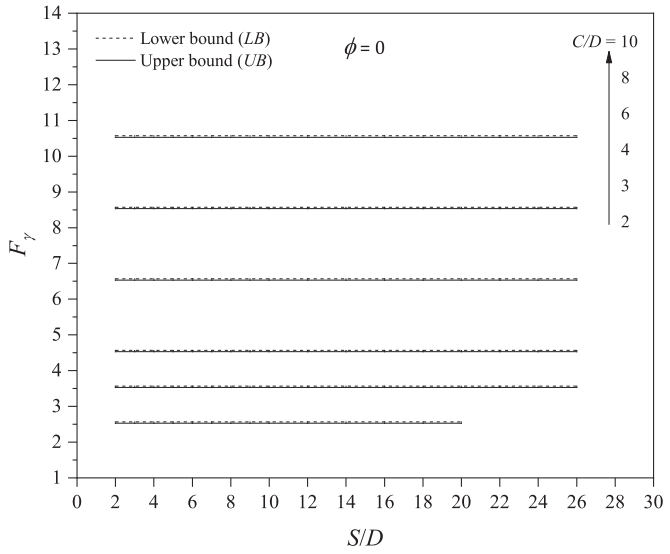

Fig. 6. 3D F_γ versus S/D and various C/D ($\phi = 0°$).

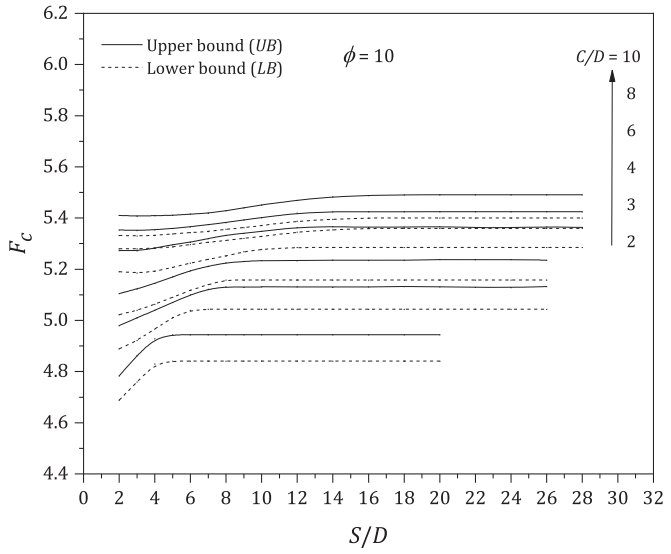

Fig. 8. 3D F_c versus S/D and various C/D ($\phi = 10°$).

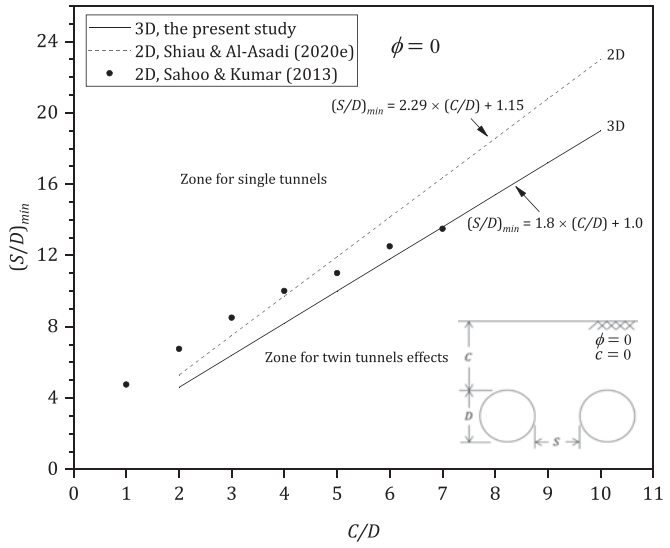

Fig. 7. Comparison of $(S/D)_{min}$.

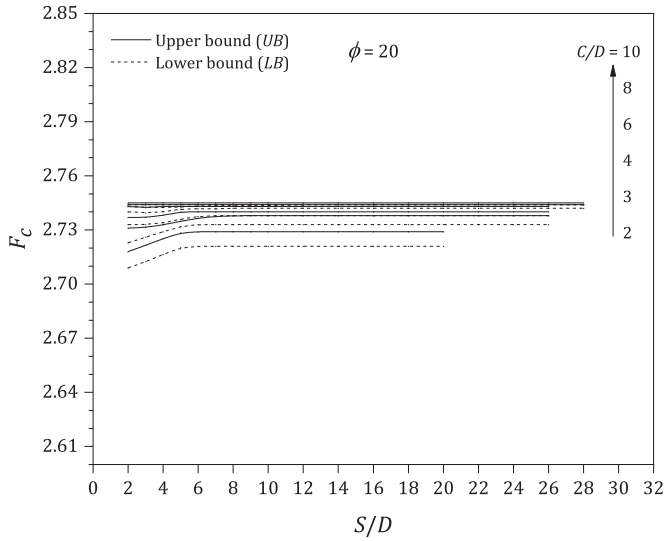

Fig. 9. 3D F_c versus S/D and various C/D ($\phi = 20°$).

F_c, F_s, and F_γ in a Drained Condition

Figs. 8–18 [for a drained condition ($\phi > 0$)] show that the three stability factors are all functions of ϕ, C/D, and S/D. Figs. 8 and 9 ($\phi = 10°$ and 20°) show that, for each C/D, F_c increased nonlinearly as S/D increased until it reached a constant value, which indicated that no interaction effect occurred between the tunnels. However, for high ϕ ($\phi \geq 20$) as shown in Figs. 10 and 11, the C/D and S/D had negligible effects on the results of F_c. This was mostly due to the development of geometrical and material arching in cohesionless soils. In general, F_c decreased as ϕ increased from 10° to 40° (Figs. 8–11).

For F_s, Fig. 12 ($\phi = 10°$) shows that F_s decreased with an increase in C/D. Of interest, note the diminishing effect of S/D on F_s when ϕ increased. This is shown in Figs. 13 to 14 ($\phi = 20°$ and $\phi \geq 25°$). Of note, F_s decreased with the increase in S/D. It then reached a constant value, although the actual F_s values (see Fig. 13) were very small. The geometrical and material arching played a major role in achieving these responses.

Finally, for F_γ, Fig. 15 ($\phi = 10°$) shows that F_γ increased with increases in C/D. It decreased with the increases in S/D until it reached a constant value. In addition, F_γ decreased dramatically with increases in ϕ (Figs. 15–18), which was due to the development of a stress arch that could carry the overburden pressure, and the tunnel stability was not directly related to the geometries (C/D and S/D). This is shown in Figs. 16–18. Of note, the values in this figure's scale are very small, the gap between UB and LB could appear to be deceptively large. In addition, F_γ had a minimum value of approximately 0.08 when $\phi = 40°$, and that the LB produced larger values of F_γ than UB, because of the active failure condition (Shiau et al. 2008). The LB is a conservative theorem that gives conservative results. The larger values of the LB would imply that a larger support pressure is required, as seen in Eq. (1), and therefore, it results in a conservative design.

Comparison of Results

FELA is most useful when UBs and LBs are calculated to bracket the true collapse load from above and below. This allows an accurate measure of the error in the solution to be computed (Sloan 2013). Figs. 4–6 and 8–18 show that the numerical UBs and LBs

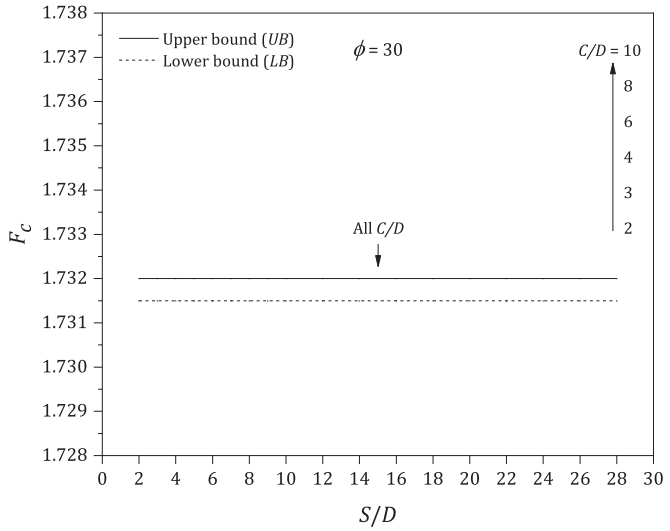

Fig. 10. 3D F_c versus S/D and various C/D ($\phi = 30°$).

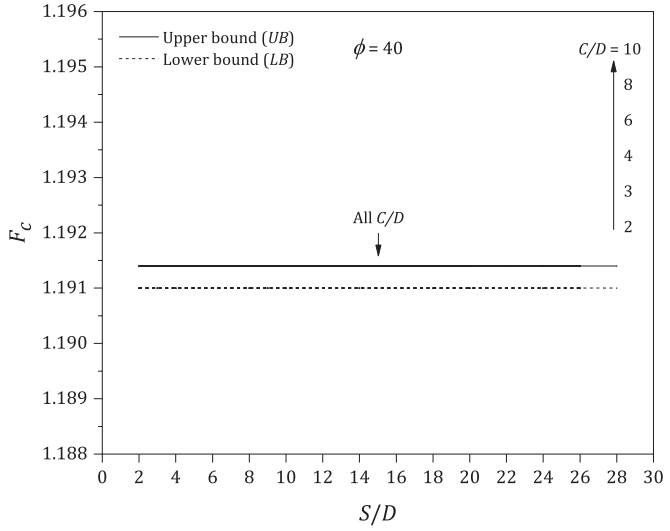

Fig. 11. 3D F_c versus S/D and various C/D ($\phi = 40°$).

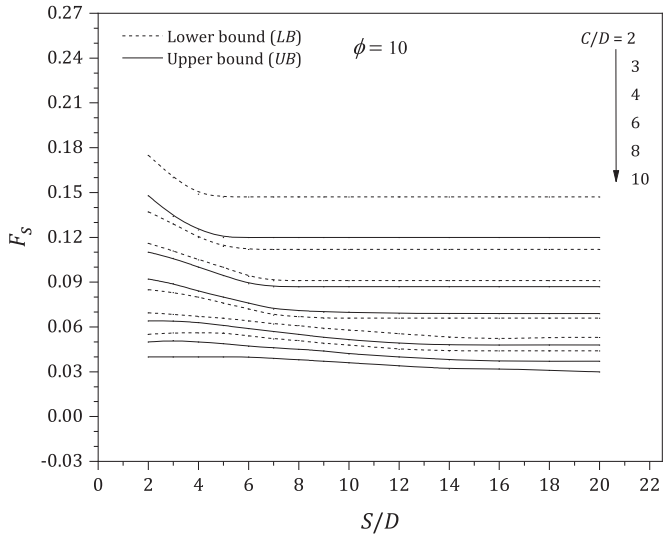

Fig. 12. 3D F_s versus S/D and various C/D ($\phi = 10°$).

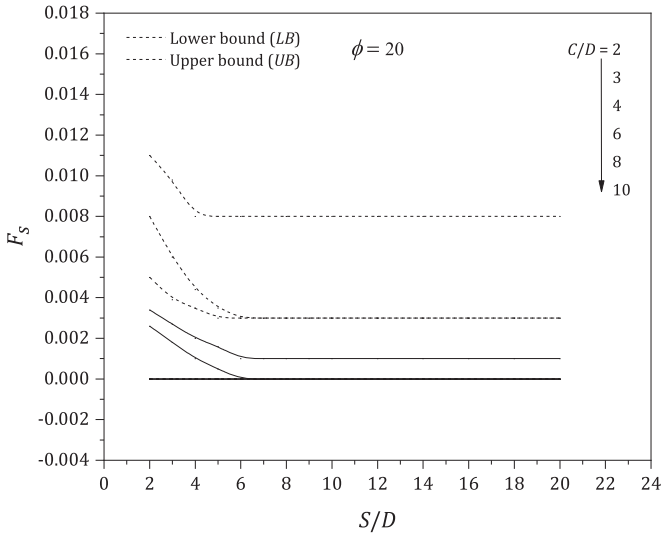

Fig. 13. 3D F_s versus S/D and various C/D ($\phi = 20°$).

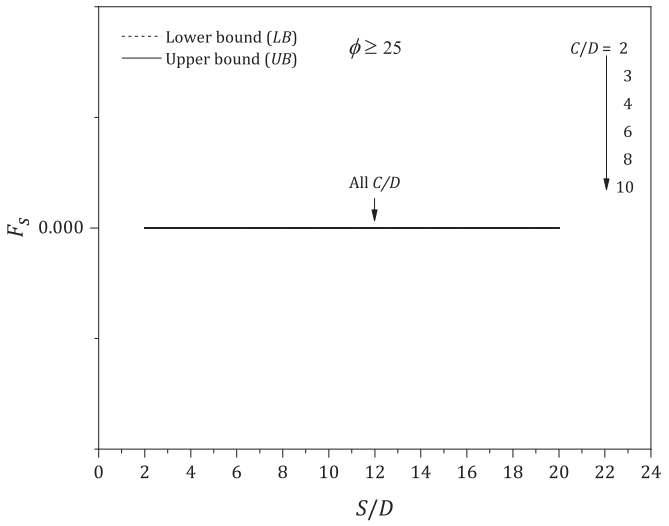

Fig. 14. 3D F_s versus S/D and various C/D ($\phi \geq 25°$).

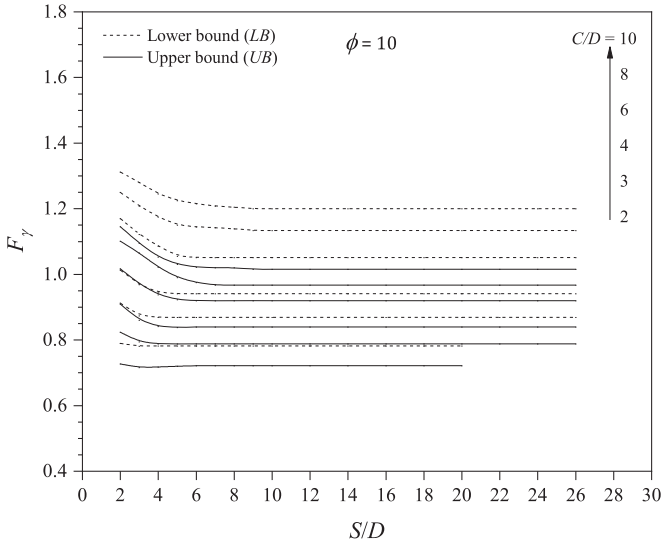

Fig. 15. 3D F_γ versus S/D and various C/D ($\phi = 10°$).

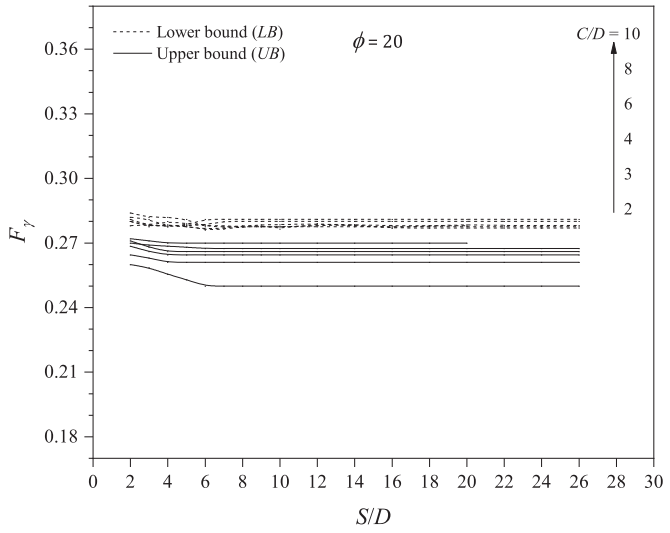

Fig. 16. 3D F_γ versus S/D and various C/D ($\phi = 20°$).

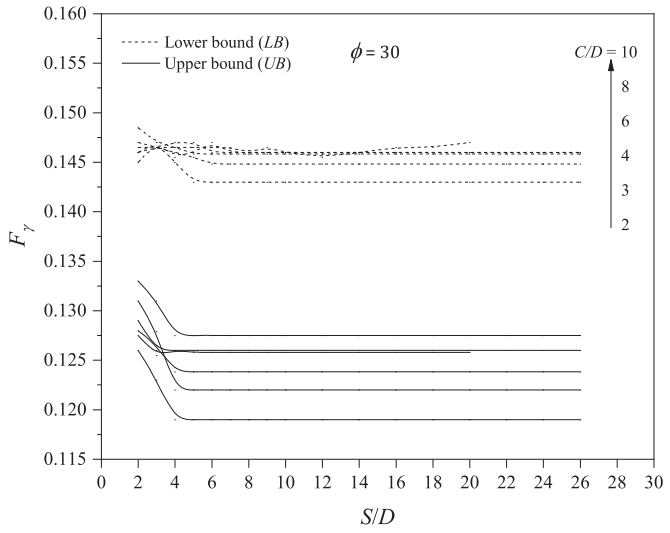

Fig. 17. 3D F_γ versus S/D and various C/D ($\phi = 30°$).

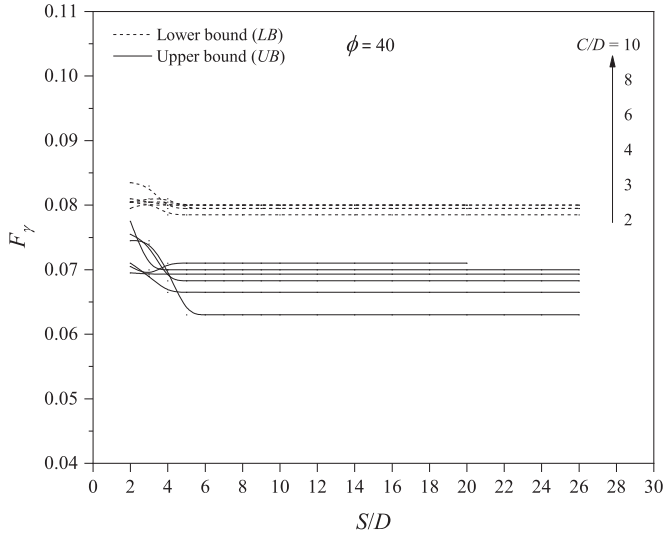

Fig. 18. 3D F_γ versus S/D and various C/D ($\phi = 40°$).

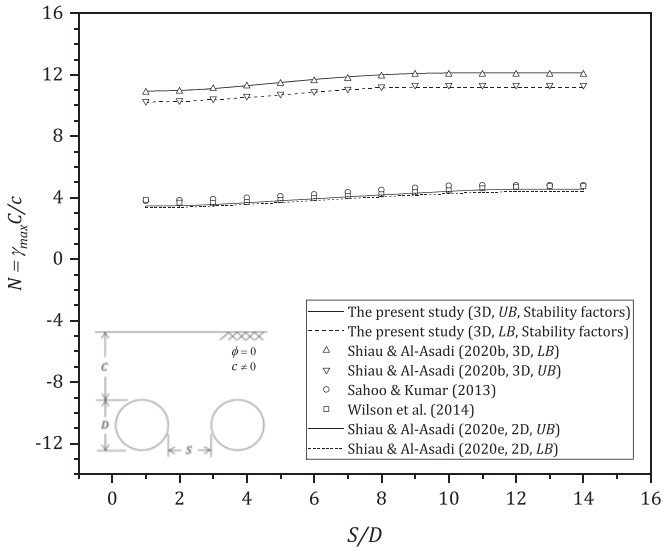

Fig. 19. Comparison of $\gamma_{max}C/c$ results with those available in the literature for twin tunnels (e.g., $C/D = 5$ and $\phi = 0°$). (Data from Sahoo and Kumar 2015.)

are generally within a few per cent of one another, with the true solution lying between both bounds. The confidence level in producing these results is extremely high although there is very little literature on 2D and 3D twin tunnels in cohesive–frictional soil.

Fig. 19 and Table 1 give a comparison between the results of this study and those from 2D undrained studies in the literature (Sahoo and Kumar 2015; Wilson et al. 2014; Shiau and Al-Asadi 2020e) and the 3D undrained studies that used Broms and Bennermarks' original stability number approach (Shiau and Al-Asadi 2020b). Fig. 19 presents excellent agreement between the 3D results of this study (stability factor approach) and the 3D undrained stability results from twin tunnels (Shiau and Al-Asadi 2020b). However, Fig. 19 shows that the variance between 3D and 2D is significant. In general, the 3D stability results were approximately three-fold higher than those in the 2D analysis. Therefore, the 2D analysis could be a conservative tool in the early stages of tunnel design. Of note, good agreement was found for all the 2D undrained results (Sahoo and Kumar 2015; Wilson et al. 2014; Shiau and Al-Asadi 2020e).

An Example

The figures and tables in this paper for the stability factors (e.g., F_c, F_s, and F_γ) were used to estimate the critical pressure to maintain the stability of the headings of 3D twin tunnels in the following example.

A twin tunnel was spaced 30 m apart (center-to-center) and the tunnels were assumed to be bored at the same time, and $D = 6.0$ m and $C = 18$ m. The soil parameter were $c = 15$ kPa, $\phi = 10°$, and $\gamma = 18$ kN/m^3. No surcharge was presented ($\sigma_s = 0$) in this example. The following procedures were used to estimate σ_t, that is, the required tunnel pressure to maintain soil stability.

1. The dimensionless ratios were calculated as: $C/D = 3$ and $S/D = 5$.
2. From Figs. 8, 12, and 15 (e.g., $C/D = 3$, $S/D = 5$, and $\phi = 10°$), the LB stability factors were $F_c = 5.01$, $F_s = 0.116$, and $F_\gamma = 0.870$.

Table 1. Comparison of $\gamma_{max}C/c$ results with those available in the literature for twin tunnels (e.g., $C/D = 5$ and $\phi = 0°$)

S/D	This study (3D, UB)	This study (3D, LB)	Shiau and Al-Asadi (2020b), (3D, UB)	Shiau and Al-Asadi (2020b), (3D, LB)	Sahoo and Kumar (2015), (2D, UB)	Wilson et al. (2014), (2D, UB)	Shiau and Al-Asadi (2020e), (2D, UB)	Shiau and Al-Asadi (2020e), (2D, LB)
1	10.93	10.22	10.85	10.27	3.79	3.86	3.47	3.36
2	10.97	10.26	10.93	10.33	3.85	3.68	3.47	3.37
3	11.10	10.37	11.09	10.45	3.91	3.65	3.55	3.46
4	11.30	10.52	11.26	10.61	3.99	3.73	3.67	3.57
5	11.50	10.68	11.43	10.76	4.09	3.84	3.80	3.69
6	11.70	10.87	11.60	10.93	4.21	3.96	3.93	3.81
7	11.88	11.05	11.76	11.08	4.35	4.09	4.06	3.95
8	12.02	11.16	11.91	11.23	4.50	4.22	4.19	4.06
9	12.10	11.19	12.02	11.33	4.65	4.35	4.30	4.17
10	12.12	11.19	12.02	11.33	4.78	4.47	4.41	4.27
11	12.12	11.19	12.02	11.33	4.81	4.60	4.52	4.36
12	12.12	11.19	12.02	11.33	4.81	4.71	4.56	4.39
13	12.12	11.19	12.02	11.33	4.81	4.76	4.56	4.40
14	12.12	11.19	12.02	11.33	4.81	4.76	4.56	4.41

Source: Data from Sahoo and Kumar (2015).

3. Using Eq. (1), σ_t was

$$\sigma_t = -cF_c + \sigma_s F_s + \gamma D F_\gamma = -15 \times 5.01 + 0 + 18 \times 6 \times 0.870 = 18.81 \text{ kPa}.$$

Therefore, what is the required critical pressure when $\phi = 20°$?

4. From Figs. 9, 13, and 16 (e.g., $C/D = 3$, $S/D = 5$, and $\phi = 20°$), the LB stability factors were $F_c = 2.73$, $F_s = 0.003$, and $F_\gamma = 0.278$.
5. Using Eq. (1), the minimum σ_t to induce collapse is $\sigma_t = -cF_c + \sigma_s F_s + \gamma D F\gamma = -15 \times 2.73 + 0 + 18 \times 6 \times 0.278 = -10.93$ kPa.
6. A negative value of σ_t indicates that the tunnel requires a pulling pressure to reach a collapsed state. Therefore, theoretically, the tunnel will remain stable without any internal pressure.

Conclusions

Very few studies have used the comprehensive stability factors approach to study 3D twin circular tunnels in cohesive–frictional soils. This paper, to the best of the authors' knowledge, is the first to investigate the problem. The following conclusions were drawn:

1. The equation to estimate the critical support pressures of 3D twin tunnels is:

$$\sigma_t = -cF_c + \sigma_s F_s + \gamma D F_\gamma$$

2. For $\phi = 0°$, F_c is directly related to the S/D and C/D, and F_s and F_γ are independent of S/D and have constant values of $F_s = 1$ and $F_\gamma = (C/D + 0.5)$, respectively.
3. For $\phi = 0°$, the stability factors are strongly related to ϕ, C/D, and S/D. In general, the three stability factors decreased as the value of ϕ increased. For $\phi \geq 20°$, the stability factors were not related to the C/D and S/D, due to the strong effect of soil arching.

The proposed tunnel stability factor approach to estimate tunnel face pressures, which is similar to the classical bearing capacity problem, could be efficient and effective for practical engineers. Great confidence is achieved when UBs and LBs are presented.

Data Availability Statement

All data, models, and codes that support the findings of this study are available from the corresponding author upon reasonable request.

References

Anagnostou, G., and K. Kovári. 1996. "Face stability conditions with earth-pressure-balanced shields." *Tunnelling Underground Space Technol.* 11 (2): 165–173. https://doi.org/10.1016/0886-7798(96)00017-X.

Atkinson, J. H., and D. M. Potts. 1977. "Stability of a shallow circular tunnel in cohesionless soil." *Géotechnique* 27 (2): 203–215. https://doi.org/10.1680/geot.1977.27.2.203.

Ghaboussi, J., and R. E. Ranken. 1977. "Interaction between two parallel tunnels." *Int. J. Numer. Anal. Methods Geomech.* 1 (1): 75–103. https://doi.org/10.1002/nag.1610010107.

Horn, N. 1961. "Horizontal earth pressure on the vertical surfaces of the tunnel tubes." In *Proc., National Conf. of the Hungarian Civil Engineering Industry*, 7–16 Budapest, Hungary: Hungarian Civil Engineering Industry. Accessed January 6, 2021. https://www.scopus.com/record/display.uri?eid=2-s2.0-75949121623&origin=inward&txGid=dba8c9a2336d33af58fb32bdeaf133ea.

Leca, E., and L. Dormieux. 1990. "Upper and lower bound solutions for the face stability of shallow circular tunnels in frictional material." *Géotechnique* 40 (4): 581–606. https://doi.org/10.1680/geot.1990.40.4.581.

Lee, C. J., B. R. Wu, H. T. Chen, and K. H. Chiang. 2006. "Tunnel stability and arching effects during tunneling in soft clayey soil." *Tunnelling Underground Space Technol.* 21 (2): 119–132. https://doi.org/10.1016/j.tust.2005.06.003.

Li, W., and C. P. Zhang. 2020. "Face stability analysis for a shield tunnel in anisotropic sands." *Int. J. Geomech.* 20 (5): 04020043. https://doi.org/10.1061/(ASCE)GM.1943-5622.0001666.

Mollon, G., D. Dias, and A.-H. Soubra. 2009. "Probabilistic analysis and design of circular tunnels against face stability." *Int. J. Geomech.* 9 (6): 237–249. https://doi.org/10.1061/(ASCE)1532-3641(2009)9:6(237).

Mollon, G., D. Dias, and A.-H. Soubra. 2010. "Face stability analysis of circular tunnels driven by a pressurized shield." *J. Geotech. Geoenviron. Eng.* 136 (1): 215–229. https://doi.org/10.1061/(ASCE)GT.1943-5606.0000194.

Mollon, G., D. Dias, and A. H. Soubra. 2011. "Rotational failure mechanisms for the face stability analysis of tunnels driven by a pressurized shield." *Int. J. Numer. Anal. Methods Geomech.* 35 (12): 1363–1388. https://doi.org/10.1002/nag.962.

Mollon, G., D. Dias, and A. H. Soubra. 2013. "Continuous velocity fields for collapse and blowout of a pressurized tunnel face in purely cohesive soil." *Int. J. Numer. Anal. Methods Geomech.* 37 (13): 2061–2083. https://doi.org/10.1002/nag.2121.

OptumCE. 2019. *OptumG3*. Copenhagen, Denmark: Optum Computational Engineering. https://optumce.com/.

Osman, A. S. 2010. "Stability of unlined twin tunnels in undrained clay." *Tunnelling Underground Space Technol.* 25 (3): 290–296. https://doi.org/10.1016/j.tust.2010.01.004.

Sahoo, J. P., and J. Kumar. 2015. "Stability of a long unsupported circular tunnel in clayey soil by using upper bound finite element limit analysis." *Proc. Indian Natl. Sci. Acad.* 79 (4): 807–815. https://doi.org/10.16943/ptinsa/2013/v79i4/48005.

Shiau, J., and F. Al-Asadi. 2018. "Revisiting Broms and Bennermarks' original stability number for tunnel headings." *Géotech. Lett.* 8 (4): 310–315. https://doi.org/10.1680/jgele.18.00145.

Shiau, J., and F. Al-Asadi. 2020a. "Three-dimensional analysis of circular tunnel headings using Broms and Bennermarks' original stability number." *Int. J. Geomech.* 20 (7): 06020015. https://doi.org/10.1061/(ASCE)GM.1943-5622.0001734.

Shiau, J., and F. Al-Asadi. 2020b. "Three-dimensional heading stability of twin circular tunnels." *Geotech. Geol. Eng.* 38 (2): 2973–2988. https://doi.org/10.1007/s10706-020-01201-z.

Shiau, J., and F. Al-Asadi. 2020c. "Two-dimensional tunnel heading stability factors F_c, F_s and F_γ." *Tunnelling Underground Space Technol.* 97: 103293. https://doi.org/10.1016/j.tust.2020.103293.

Shiau, J., and F. Al-Asadi. 2020d. "Determination of critical tunnel heading pressures using stability factors." *Comput. Geotech.* 119: 103345. https://doi.org/10.1016/j.compgeo.2019.103345.

Shiau, J., and F. Al-Asadi. 2020e. "Stability analysis of twin circular tunnels using shear strength reduction method." *Geotech. Lett.* 10 (2): 311–319. https://doi.org/10.1680/jgele.19.00003.

Shiau, J., and F. Al-Asadi. 2020f. "Twin tunnels stability factors F_c, F_s and F_r." *Geotech. Geol. Eng.* 39 (1): 1–11. https://doi.org/10.1007/s10706-020-01495-z.

Shiau, J., and F. Al-Asadi. 2021. "Revisiting circular tunnel stability using Broms and Bennermarks' original stability number." *Int. J. Geomech.* 21 (5): 06021009. https://doi.org/10.1061/(ASCE)GM.1943-5622.0001996.

Shiau, J., B. Chudal, K. Mahalingasivam, and S. Keawsawasvong. 2021a. "Pipeline burst-related ground stability in blowout condition." *Transp. Geotech.* 29: 100587. https://doi.org/10.1016/j.trgeo.2021.100587.

Shiau, J., and M. M. Hassan. 2020. "Undrained stability of active and passive trapdoors." *Geotech. Res.* 7 (1): 40–48. https://doi.org/10.1680/jgere.19.00033.

Shiau, J., B. Lamb, and M. Sams. 2016. "The use of sinkhole models in advanced geotechnical engineering teaching." *Int. J. Geomate* 10 (2): 1718–1724.

Shiau, J., J.-S. Lee, and F. Al-Asadi. 2021b. "Three-dimensional stability analysis of active and passive trapdoors." *Tunnelling Underground Space Technol.* 107: 103635. https://doi.org/10.1016/j.tust.2020.103635.

Shiau, J., and M. Sams. 2019. "Relating volume loss and greenfield settlement." *Tunnelling Underground Space Technol.* 83: 145–152. https://doi.org/10.1016/j.tust.2018.09.041.

Shiau, J. S., C. E. Augarde, A. V. Lyamin, and S. W. Sloan. 2008. "Finite element limit analysis of passive earth resistance in cohesionless soils." *Soils Found.* 48 (6): 843–850. https://doi.org/10.3208/sandf.48.843.

Sloan, S. W. 2013. "Geotechnical stability analysis." *Géotechnique* 63 (7): 531–572. https://doi.org/10.1680/geot.12.RL.001.

Ukritchon, B., K. Yingchaloenkitkhajorn, and S. Keawsawasvong. 2017. "Three-dimensional undrained tunnel face stability in clay with a linearly increasing shear strength with depth." *Comput. Geotech.* 88: 146–151. https://doi.org/10.1016/j.compgeo.2017.03.013.

Ukritchon, B., S. Yoang, and S. Keawsawasvong. 2020. "Undrained stability of unsupported rectangular excavations in non-homogeneous clays." *Comput. Geotech.* 117: 103281. https://doi.org/10.1016/j.compgeo.2019.103281.

Wilson, D. W., A. J. Abbo, S. W. Sloan, and A. V. Lyamin. 2014. "Undrained stability of dual circular tunnels." *Int. J. Geomech.* 14 (1): 69–79. https://doi.org/10.1061/(ASCE)GM.1943-5622.0000288.

Wilson, D. W., A. J. Abbo, S. W. Sloan, and A. V. Lyamin. 2015. "Undrained stability of dual square tunnels." *Acta Geotech.* 10 (5): 665–682. https://doi.org/10.1007/s11440-014-0340-1.

Wu, B. R., and C. J. Lee. 2003. "Ground movements and collapse mechanisms induced by tunneling in clayey soil." *Int. J. Phys. Modell. Geotech.* 3 (4): 15–29. https://doi.org/10.1680/ijpmg.2003.030402.

Zhang, C. P., K. H. Han, and D. L. Zhang. 2015. "Face stability analysis of shallow circular tunnels in cohesive-frictional soils." *Tunnelling Underground Space Technol.* 50: 345–357. https://doi.org/10.1016/j.tust.2015.08.007.

Zhang, C. P., W. Li, W. J. Zhu, and Z. B. Tan. 2020. "Face stability analysis of a shallow horseshoe-shaped shield tunnel in clay with a linearly increasing shear strength with depth." *Tunnelling Underground Space Technol.* 97: 103291. https://doi.org/10.1016/j.tust.2020.103291.